RSC Advances

ROYAL SOCIETY OF CHEMISTRY

www.rsc.org/advances

Journal Name

RSCPublishing

ARTICLE

Designed hierarchical MnO_2 microspheres assembled by nanofilms for removal of heavy metal ions

Cite this: DOI: 10.1039/x0xx00000x

Yuanyuan Guo[a], Hong Guo* [a, b], Yapeng Wang[a], Lixiang Liu[a] and Weiwei Chen[a]

Received 00th January 2012,
Accepted 00th January 2012

DOI: 10.1039/x0xx00000x

www.rsc.org/

Hierarchical MnO_2 microspheres assembled by nanofilms are fabricated through an environmental route and subsequent dry under vacuum. Adsorption kinetics and thermodynamics are investigated in detail. The unique nanofilm assembly structure with high BET surface area of 252.82 m^2g^{-1} can allow for higher exposure of adsorption sites to adsorbate molecules than a solid one, and thus results in the high removal efficiency of heavy metal ions. The final removal efficiency of Pb (II), Cd (II), Cu (II) and Cr (VI) from acid aqueous solutions can arrive at 100%, 99.6%, 99.1% and 95.2%, respectively. Moreover, the relative large submicrometer particles are easy to be recovered after adsorption. Therefore, it may serve as an ideal candidate for heavy metal ions removal in water treatment.

Introduction

Heavy metal ions, unlike organic contaminants, have become an ecotoxicological hazard of prime interest and increasing significance because which once emitted can reside in the environment for hundreds of years or more and tend to accumulate in living organisms[1-3]. Among the known heavy metals, lead is an industrial pollutant, and contamination of water resources by lead is one of the most serious problems for public health and the environment. The major sources are from a variety of industrial wastes, such as electroplating, manufacturing of batteries, pigments and ammunition. Human exposure to lead can occur via food, air, soil and dust,[4,5] and lead is linked to reproductive and nervous system problems, high blood pressure, kidney damage, memory and concentration difficulties in high amounts, coma, convulsions and death. Therefore, this element must be removed from wastewater prior to discharge. The normal techniques for heavy metals removal from water effluents are: ion exchange, coagulation-precipitation, electro-dialysis, filtration, electro-chemical precipitation, reverse osmosis, evaporation, chemical precipitation and adsorption.[6,7] The major drawbacks with these processes are high cost, toxic sludge generation or incomplete metal removal. [8-10]

Most recently, manganese oxides have attracted great interest and been demonstrated adsorption and catalytic properties suitable for using in environmental remediation[11], catalysis,[12] sensors,[13] and energy storage[14] due to the existence of unique layers or tunnels in crystal lattices, low cost, high activity/stability, high specific surface areas, and environmental compatibility. [15-20] Many efforts have been focused on synthetic procedures for manganese oxides including laser ablation, sonochemical methods, hydrothermal methods and synthesis using polyelectrolytes. In the past decades, for the sorption by manganese dioxide of cationic or anionic pollutants, such as heavy metal ions, organic contaminants like substituted phenols, dyes, aromatic amines, explosives and pesticides[21,22] from natural waters has attracted considerable attention, because it would significantly mediate the fate and mobility of the targeted pollutants in water[23]. For example, Chen and co-workers[24] synthesised porous MnO_2 microspheres for the adsorption of methyl blue. Especially, Kanungo et al.[25] found that some toxic metals (Co(II), Ni(II), Cu(II), and Zn(II) ions) can be effectively trapped by manganese dioxide through electrostatic forces and formation of inner-sphere complexes, which rendered it a potential sorbent for heavy metal removal from contaminated waters. Fan and co-workers[26] used hydrous manganese dioxide as a potential sorbent for selective removalof lead, cadmium, and zinc ions from water. Kim and co-workers[27] prepared hierarchical MnO_2-coated magnetic nanocomposite with good performance for removing heavy metal ions from contaminated water systems.These results prompt us to carry out the corresponding work on removal of heavy metal ions from wastewater.

Furthermore, controlling crystal phase, particle size, crystallinity, morphology of manganese oxides have been proved to be an efficient and innovating solution to environmental problems.[28-33] Nanosized manganese oxides are one of the most reactive minerals that have high surface area, strong oxidizing/adsorptive abilities, and good stability under acidic conditions.[26,27,33] Especially, the thin film structures at the nano scale are attracting fast growing interest because they can be used to find new applications owing to their specific geometry and structural flexibility.[34–38] Up to now, the common synthetic strategy for the fabrication of those structures with complex interiors employs sacrificial templates, such as polymer, silica, carbon inorganic spheres and ionic liquids. However, templating methods for constructing complex nanostructures are usually time consuming and costly because of the need for the synthesis of the templates and the multi-step templating process, and thus it is highly desirable to develop facile, scalable approaches for the rational synthesis of those structures with designed interior structures. Therefore, a general approach of rationally fabricating microspheres assembled by

nanofilms for removal of heavy metal ions is still lacking and it is desirable to obtain these materials through more facile, economic and environment-friendly process. Besides, an advantage for chemists is to elaborate possible new constructions from all chemical components without any time-restricted conditions.

Herein, we chose MnO_2 to demonstrate our concept and propose a facile generic strategy to prepare microspheres assembled by nanofilms with a high purity, high surface areas, and enhanced adsorption activity for the removal of heavy metal ions. Compared with conventional template-assisted methods, MnO_2 materials prepared as such have relatively lower density, higher surface area and more stable configuration without the destructive effect of template removal on product morphology. To our best knowledge, the fabrication of MnO_2 microspheres assembled by nanofilms and the adsorption mechanism of Pb^{2+} on manganese dioxides have never been reported previously. Hence, a higher degree of metal utilization as enhanced performance for removal of heavy metal ions can be expected. Additionally, this route is environmentally friendly, mass-productive and low cost.

Experimental

Synthesis of MnO_2 microspheres assembled by nanofilms

In a typical synthesis process, 0.28 g of $KMnO_4$, 0.01 g of $NH_4H_2PO_4$ and 0.01 g of $Na_2SO_4{\cdot}10H_2O$ were dissolved by a specific amount of distilled water respectively then mixed together and subsequently distilled water was added to the mixture to keep the final volume at 90 mL. The solution above was agitated with a magnetic stirrer for 15 min, then the mixture was transferred into a Teflon-lined stainless steel autoclave with a capacity of 100 mL for hydrothermal treatment at 140 °C for 48 h. As the autoclave cooled down to room temperature, the gray precipitate was harvested by several rinse-centrifugation cycles with deionized water and absolute ethanol, and finally dried under vacuum at 70 °C overnight for further characterization.

Characterization

X-ray diffraction (XRD) was carried out to identity the phase composition of synthesized samples over the 2θ range from 20° to 90° using a Rigaku D/max-A diffractometer with Co Kα radiation. A Fourier transform infrared spectroscope (FTIR, Themo Nicolet 670FT-IR) was used for recording the FTIR spectra of the sample ranged from 400 to 4000 cm^{-1}. Morphologies of the synthesized samples were observed with a AMRAY 1000B scanning electron microscope (SEM), and the microstructural characteristics of samples were observed by high-resolution transmission electron microscope (HR-TEM, JEOL JEM-2100) working at 200 kV accelerating voltage and the lattice structure was identified by selected area electron diffraction (SAED) technique. Nitrogen adsorption-desorption measurements were conducted at 77 K on a Micromeritics Tristar apparatus. Specific surface areas were determined following the Brunauer-Emmet-Teller analysis. Atomic adsorption spectroscopy (AAS) analyses, on a S4 Thermo Electron spectrometer equipped with hollow cathode lamps and an acetylene-air flame, were used for quantitation.

Heavy metal ion removal experiments

The removal experiments of heavy metal ions were carried out at room temperature. Firstly, the adsorption solutions of Pb (II), Cd (II), Cu (II) and Cr (VI) were prepared by adding a certain amount of original heavy metal ion solutions in four closed vessels respectively, and then a mixed solution of 0.1 M HCl and 0.1 M $NH_3{\cdot}H_2O$ was added to adjust the pH value to 3. And finally the volume the adsorption solutions of Pb (II), Cd (II), Cu (II) and Cr(VI) was 100 mL with the concentrations of 10 $mg{\cdot}L^{-1}$ respectively. Then 20 mg of the sample was added to the solutions above, and stirred for 24 h. During the adsorption process, at different periods (0, 0.5, 1, 1.5, 2, 4, 6, 10, and 24 h), about 0.2 mL of each solution above was extracted with a needle tube equipped with a membrane filter and then diluted to be used for AAS measurements.

Results and discussion

Structure and morphology of MnO_2 microspheres assembled by nanofilms

The XRD patterns of the synthesized MnO_2 microspheres assembled by nanofilms as shown in Fig. 1, declare a tetragonal a-MnO_2 structure (JCPDS card No. 44-0140, a = 0.978 nm, c = 0.285 nm) of the synthesized sample. No other peaks are identified, which indicates a good purity of the samples. Detailed analysis of the peak broadening of the (3 1 0) reflection using the Scherrer equation indicates an average crystallite size ca. 3 nm, suggesting that these MnO_2 particles are composed of nanocrystal subunits.

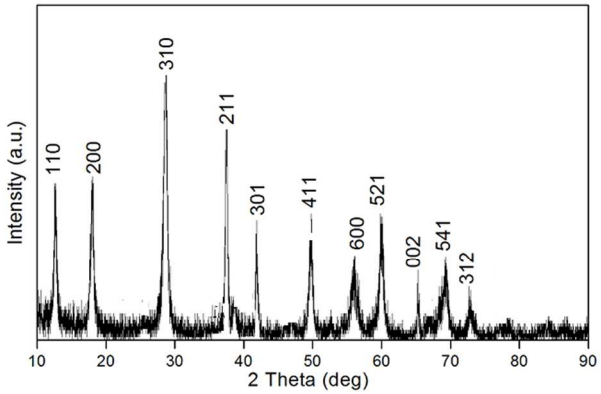

Fig. 1 XRD pattern of MnO_2 (JCPDS card No.44-0140) microspheres assembled by nanofilms.

SEM image of the MnO_2 microspheres assembled by nanofilms is shown as Fig. 2a, which illuminates the as-synthesized samples are uniform microspheres with an average size of ca. 700 nm. It is interesting to find that the obtained MnO_2 powder is made up from thin nanosheets. The unique morphology of MnO_2 samples is also characterized by TEM and HR-TEM, as illustrated in Fig. 2b-e. Fig. 2b shows the resulting MnO_2 microspheres are visible nano thin flim assembly obviously, which is consistent with the SEM analysis. Fig. 2c confirms that the relatively large particle is aggregates of thin nanosheets, and its thickness is as thin as 2-3 nm accoding to Fig. 2d. The detected lattice spacing of 0.311 nm agrees with tetragonal a-MnO_2 (3 1 1) plane spacing from Fig. 2e. The selected area electron diffraction (SAED) pattern is displayed in Fig. 2f, revealing the diffraction rings 1-3 are indexed to (2 0 0), (3 1 0) and (2 1 1) diffraction of tetragonal a-MnO_2, respectively. It indicates that the MnO_2 is composed of fine crystal particles with partial orientation. These results are in total agreement with the observed XRD analysis. The unique hierarchical nanofilm assembly structure would allow higher exposure efficiency of adsorption site to the adsorbate than a solid one, and thus is expected to be favorable for enhanced absorbtion activity for removal of heavy metal ions.

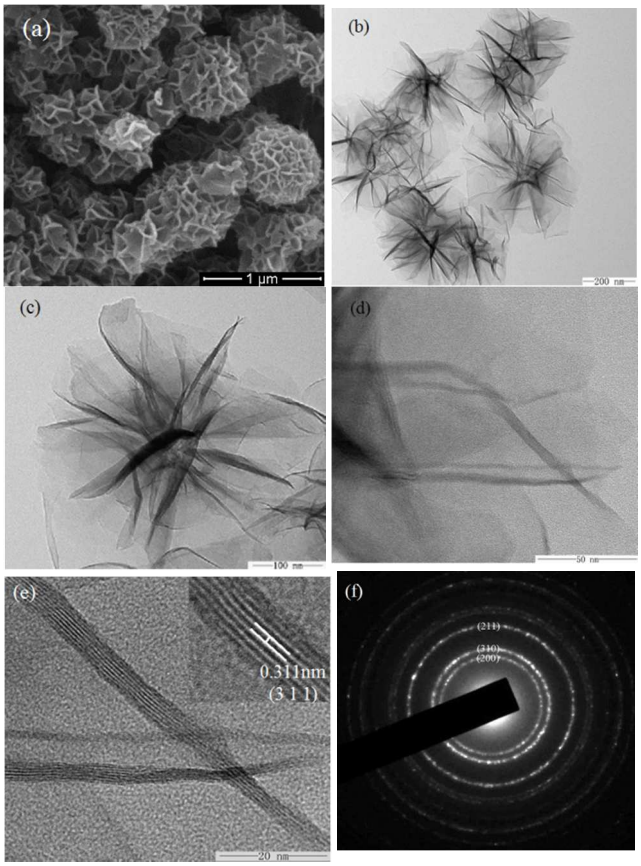

Fig. 2 SEM (a), TEM (b, c, d) images, HRTEM micrographs (e), and selected area electron diffraction (f) of as-synthesized MnO_2 samples, which is yielded by solvothermal reaction at 140 °C for 48 h, and subsequent dried under vacuum at 70 °C overnight.

The N_2 adsorption/desorption isotherms and the pore size distribution of the obtained MnO_2 samples is shown as Fig. 3. The isotherm is identified as type IV, which is the characteristic isotherm of mesoporous materials. The pore size distribution data indicates that average pore diameters of the product are in the range of 3.2-7.5 nm. The BET surface area of the sample is 252.82 m^2g^{-1}, which is high than most reports.[24,25,26,27] The single-point total volume of pores at $P/P_0 = 0.975$ is 0.202 cm^3g^{-1}. The BET surface area and the large total pore volume strongly indicate that the prepared MnO_2 products have a loose mesoporous structure, which is benefit for the enhanced adsorption performance.

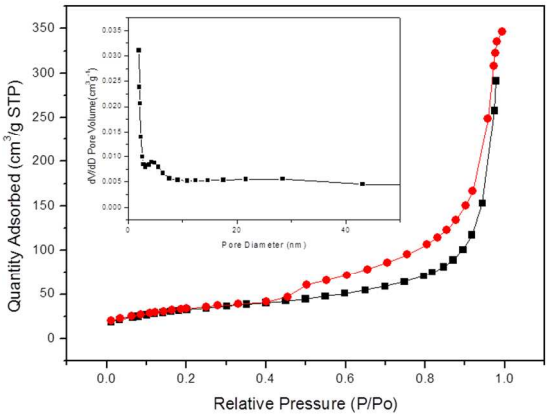

Fig. 3 Nitrogen adsorption–desorption isotherm and Barrett–Joyner–Halenda (BJH) pore size distribution plot (inset) of the prepared MnO_2 samples.

Adsorption capacity

The adsorption capacity of MnO_2 sample for removing heavy metal ions of Pb (II), Cd (II), Cu (II) and Cr (VI) from acid aqueous solutions (pH = 3) at room temperature are investigated by conducting a series of kinetic experiments as shown in Fig. 4. It can be seen that all the adsorption ions can be well adsorbed with final removal efficiency of 100%, 99.6%, 99.1% and 95.2% corresponding to Pb (II), Cd (II), Cu (II) and Cr (VI), respectively. The intrinsic hierarchical microstructure assembled by nanofilms with high specific surface areas provides MnO_2 with more active site, and thus results in the high removal efficiency of heavy metal ions. Moreover, the relative large submicrometer particles are easy to be recovered after adsorption.

The removal rates of Cd (II), Cu (II) seem not good than that of Pb (II). This is reasonable because the adsorption for heavy metal ions usually occur via ion-exchange, and electrostatic interaction between free metal ions and the surface of the samples in solutions. So, the Pb (II) is heavy and not easy desorption after ion-exchange compared with relative light element of Cd, Cu and Cr.[39-45] To identify the interaction between MnO_2 samples and heavy metal ions during the adsorption process, the FTIR spectra of the sample with the highest adsorption capacity of Pb^{2+} before and after adsorption is shown in Fig. 5 as curve a and b, respectively. The broad vibration band (ca. 3426 cm^{-1}) is attributed to the stretching vibration of the –OH group from H_3O^+ formed by ion exchange reactions or physical adsorption water molecules. The peak at 2320.54 cm^{-1} is from the stretching vibration of CO_2. While the peak at ca. 1630 cm^{-1} and 1401 cm^{-1} can be normally associated with the O–H bending mode. The strongest broad peaks in the range of 400-1000 cm^{-1} are contribution from O-metal bonds. The peak at around 530 cm^{-1} is from manganese oxides.[46–48] The peak intensity and position of Metal-O bond has a little discrepancy before and after adsorption of Pb^{2+}, implying Pb^{2+} sticks on the MnO_2 strongly.

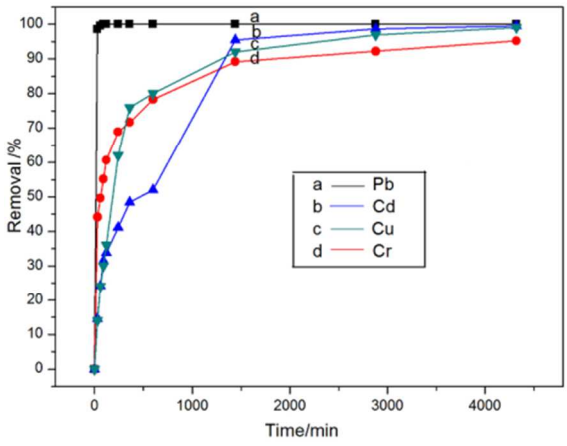

Fig. 4 Relationship between the removal efficiency and time for the adsorption of Pb (II), Cd (II), Cu (II) and Cr (VI) by MnO_2 (200 $mg \cdot L^{-1}$) sample at initial concentrations of heavy metal ions of 10 $mg \cdot L^{-1}$, respectively.

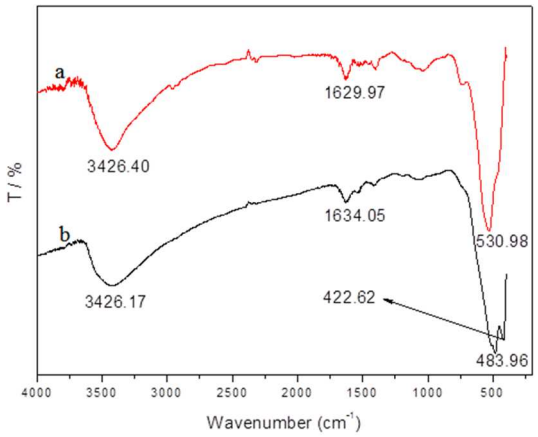

Fig. 5 FTIR spectra of the prepared MnO_2 sample before (a) and after (b) adsorption of Pb (II).

Adsorption kinetics

For investigation of the adsorption capacity and kinetics of the MnO_2 microspheres assembled by nanofilms, Pb^{2+} is chosen for removing from acid aqueous solutions (pH = 3). With different initial solution concentrations of 10, 30 and 50 mg·L^{-1}, the solution volume of 100 mL, and adsorption temperature of 30℃, 10 mg adsorbent was added to a series of 250 mL conical flasks with Pb^{2+} solutions respectively. During the adsorption process, at different periods of 0, 7, 14, 21, 28, 35, 60, 180, 480, and 1440 min, about 1 mL of each solution above was extracted using a needle tube equipped with a membrane filter and then diluted to be used for AAS measurements. The adsorption kinetics of MnO_2 sample could be perfectly fitted by a pseudo-second-order model expressed by eqn (1), (2) and (3):

$$\frac{t}{q_t} = \frac{1}{k_2 q_e^{\ 2}} + \frac{t}{q_e} \quad (1)$$

$$q_t = \frac{(C_0 - C_t)V}{W} \quad (2)$$

$$q_e = \frac{(C_0 - C_e)V}{W} \quad (3)$$

where, q_e and q_t (mg·g^{-1}) are the amounts of Pb^{2+} adsorbed on unit mass of the adsorbent when the concentration is equilibrium and at time t (min), respectively; k_2 (g·mg^{-1}·min^{-1}) is the rate constant of the pseudo-second-order kinetic model. C_0 , C_e and C_t (mg·L^{-1}) are the concentrations of Pb (II) initially, at equilibrium and any time t, respectively, V is the volume of the Pb (II) solution (L), and W is the mass of adsorbent added (g). Fig. 6a shows the effectiveness of MnO_2 sample in Pb^{2+} removal at three initial concentrations of 10, 30 and 50 mg·L^{-1} as a function of reaction time at 30 °C. This result reveals the MnO_2 microspheres assembled by nanofilms possessed super adsorption performance and good separability. Fig. 6b shows the plot of adsorption rate as a function of different concentrations of Pb^{2+} (10, 30 and 50 mg·L^{-1}). As observed that the adsorption rate of Pb^{2+} removal by MnO_2 is related to its initial concentration, and with the lower concentration, the adsorption rate turns out to be the faster. This could be explained by a mechanism that involved specific metal ion adsorption at a limited number of surface active sites. In other words, with the increase of the Pb^{2+} concentration, the high energy sites were firstly saturated and then adsorption started on low energy sites, resulting in the decrease in the adsorption rate.[49,50] Based on the data of the Pb^{2+} adsorption equilibrium and kinetics of MnO_2 listed in Table 1, all the obtained correlation coefficient R^2 are 0.999, which indicates that the pseudo-second-order model can represent the adsorption kinetics experimental data well.

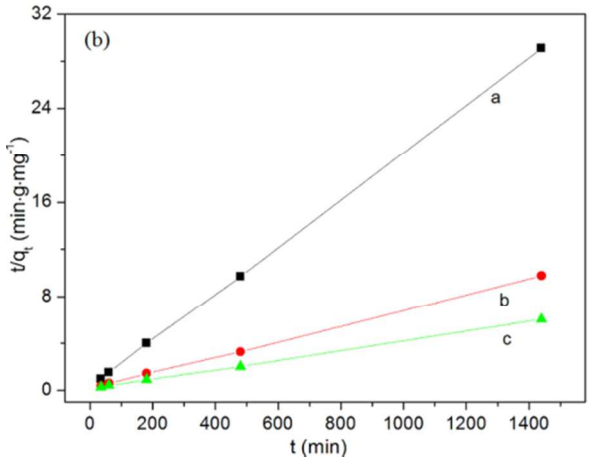

Fig. 6 (a) Relationship between the removal efficiency and time for the adsorption of Pb (II) by MnO_2 (10 mg) at initial Pb^{2+} concentrations of 10 mg·L^{-1}, 30 mg·L^{-1}, 50 mg·L^{-1}. (b) Pseudo-second-order kinetics for adsorption of Pb^{2+} on the MnO_2 sample (T=30°C; absorbent dose=100mg·L^{-1}; Pb^{2+} concentrations : a=10 mg·L^{-1}, b=30 mg·L^{-1}, c=50 mg·L^{-1}).

Table 1 The fitted parameters for equilibrium and kinetic adsorption of Pb (II) by MnO_2 sample

Sample	$[Pb(II)]_0$ (mg/L)	$q_{e,exp}$ (mg / g)	$q_{e,cal}$ (mg / g)	$k_2\times10^{-3}$ (g·mg^{-1}·min^{-1})	R^2	%E (24 h)
MnO_2	10	49.50	50.00	1.46	0.999	99.5
	30	147.00	149.25	0.29	0.999	98.7
	50	237.50	243.90	0.12	0.999	95.2

Adsorption isotherms

To conduct the adsorption isotherm experiments, a suitable amount of adsorbent (10 mg) was added to a series of 250 mL conical flasks with Pb^{2+} solutions (100 mL, 10-60 mg·L^{-1}, pH = 3). Subsequently, the sealed conical flasks were placed in a thermostatic shaker for 24 hours at 150 rpm and kept the temperature at 30°C. Then the supernatant solution was separated from the adsorbent by centrifugation, and measured by the AAS. Adsorption capacity of the MnO_2 samples for Pb^{2+} at 30°C can be obtained by the adsorption isotherms (Fig.7a). The adsorption process can be explained by the Langmuir and Freundlich isotherms. According to the Langmuir equation that the adsorption is localized in a monolayer and there is no interaction between the adsorbate molecules[51]. Besides, once a site was occupied by adsorbate molecules, no further adsorption can take place at that site. The linear form of the Langmuir isotherm is given as follows:

$$\frac{C_e}{q_e} = \frac{C_e}{q_{max}} + \frac{1}{k_L q_{max}} \quad (4)$$

Where q_{max} is the theoretical maximum monolayer sorption capacity (mg·g^{-1}), k_L is the Langmuir constant (L·mg^{-1}). However, the results

are not fitted well with the Langmuir isotherms according to our analysis. The Freundlich isotherm is another common empirical model corresponding to linear form as eqn (5), which is supposed that the stronger binding sites are first occupied and the binding strength decreases with the increasing of the site occupation degree. [52]

$$\lg q_e = \lg k_F + \frac{1}{n}\lg C_e \qquad (5)$$

Where k_F and 1/n are the Freundlich constant $(mg\cdot g^{-1})(L\cdot mg^{-1})^{1/n}$ and the heterogeneity factor, respectively. Fig.7b shows the detailed information of the constant k_F and 1/n which can be determined by a plot of lg q_e *versus* lg C_e. The Freundlich exponent n is greater than 1 from Table 2, suggesting an advantageous adsorption condition. [52,53] It indicates that heterogeneity on the surfaces or pores of the MnO_2 sample plays a key role in Pb^{2+} adsorption. Moreover, the correlation coefficient R^2 of the sample is as high as 0.9915 as shown in Table 2, which confirms that Freundlich isotherm model is in good agreement with the experimental equilibrium analysis.

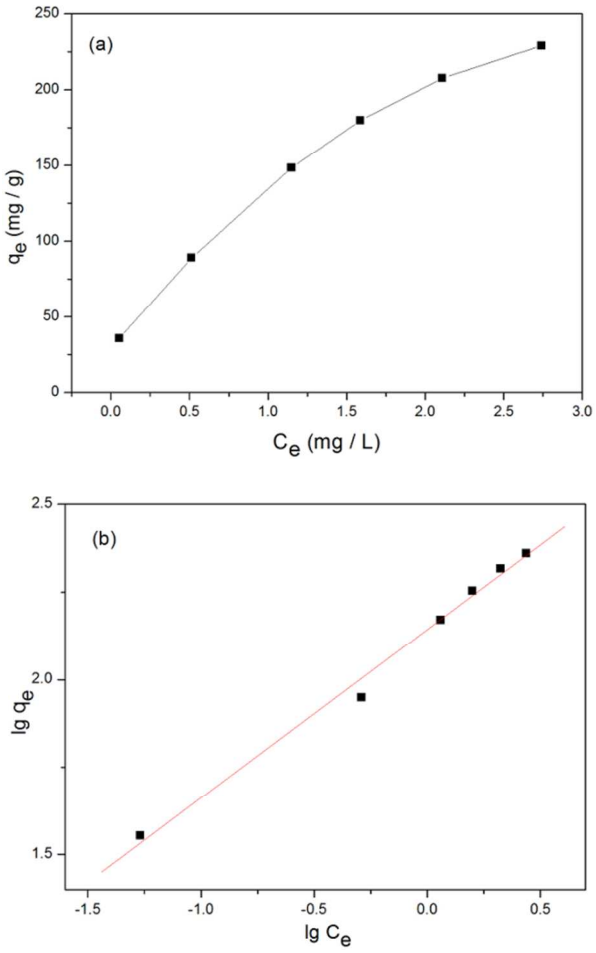

Fig.7 (a) Adsorption isotherm for Pb^{2+} on the MnO_2 sample (T=30 °C; adsorbent dose=100 $mg\cdot L^{-1}$; Pb^{2+} concentration=10-60 $mg\cdot L^{-1}$). (b) Freundlich linear plots for adsorption isotherm of the MnO_2 sample on removal of Pb^{2+} at 30 °C.

Table 2 Freundlich isotherm parameters of the MnO_2

Sample	k_F $(mg\cdot g^{-1})$ $(L\cdot mg^{-1})^{1/n}$	n	R^2
MnO_2	139.28	2.07	0.9915

Adsorption thermodynamics

The thermodynamics analysis was carried out according to Arrhenius equation (equ 6) under certain assumption of an isolated system[54,55]. In a typical experiment, with the initial concentration of 30 $mg\cdot L^{-1}$, the adsorption volume of 100 ml, 10 mg adsorbent was added to the Pb^{2+} solutions contained in 250 mL conical flasks at three temperatures (30°C, 40°C and 50°C), respectively. At different time intervals, the aqueous samples were sampled and the corresponding concentrations of Pb^{2+} were similarly measured through AAS to study the adsorption kinetics of Pb^{2+} at different temperatures. The Arrhenius equation has been applied to measure the activation energy, which is a threshold for the adsorption reaction.

$$\ln k_2 = \ln A - \frac{E_a}{RT} \qquad (6)$$

where E_a, A, R, T are the Arrhenius activation energy $(kJ\cdot mol^{-1})$, the Arrhenius factor, the gas constant (8.314 $J\cdot mol^{-1}\cdot K^{-1}$) and the absolute temperature (K), respectively. A straight line with the slope -Ea/R is obtained, when $\ln k_2$ is plotted against 1/T (Fig. 8). The type of adsorption can be judged by the magnitude of activation energy. The activation energies of physisorption processes is often in the range of 0–40 $kJ\cdot mol^{-1}$, while higher activation energies (40–800 $kJ\cdot mol^{-1}$) implying chemisorption.[54] The value of the activation energy is 28.08 $kJ\cdot mol^{-1}$, revealing the adsorption process of Pb^{2+} onto the MnO_2 is belong to physisorption.

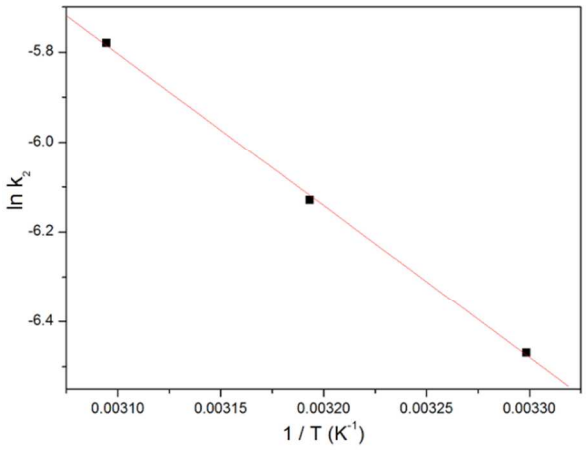

Fig. 8 Plot of $\ln k_2$ *versus* 1/T for Pb^{2+} adsorption on the MnO_2 sample.

Conclusions

Hierarchical MnO_2 microspheres assembled by nanofilms are successfully synthesized by a facile and environmentally benign procedure combining with solvothermal synthesis. The unique nanofilm assembly structures allow for higher exposure of adsorption sites to adsorbate molecules than a solid one, and thus it exhibits a remarkable adsorption activity for removal of heavy metal ions. This strategy is simple, cheap and mass-productive, which may shed light on a new avenue for large-scale synthesis of hierarchical nano/micro functional materials for environmental remediation, catalyst, energy and other applications.

Acknowledgements

The authors would like to acknowledge financial support provided by Department Science Foundation of China (No.210204), National Natural Science Foundation of China (No.U0937601), 863 Program of National High Technology Research Development Project of China (No. 2011AA03A405) and Major state basic research revelopment program of China (973 Program, No. 2014CB643406).

Notes and references

[a] School of Chemistry Science and Engineering, Yunnan University, Kunming 650091,Yunnan, China. Fax: +86-871-65036626; Tel: +86-871-65032180; E-mail: guohongcom@126.com

[b] School of Chemistry Science and Engineering, Qujing Normal University, Qujing 65500, Yunnan, China

Electronic Supplementary Information (ESI) available: [details of any supplementary information available should be included here]. See DOI: 10.1039/b000000x/

1 R. Krmer, *Angew. Chem.*, 1998, **110**, 804.
2 H. Lee, D. Bae, J. Park, H. Song, W. Han and Jung, *Angew. Chem.*, 2009,**121**, 1265.
3 A. Shahbazi, H. Younesi, and Badiei, *J. Chem. Eng.*, 2013,**91**,739.
4 M. R. Krigman, *Environ. Health. Perspect.*, 1978, **26**,117.
5 J. M. Davis, *Neurotoxicology*, 1990,**11**, 285.
6 M. H. Karaoglu, S. Zor, M. Ug˘urlu, *J. Chem. Eng.*, 2010, **159**, 98.
7 V. K. Gupta, V. K. Saini, N. Jain, *J. Colloid Interface Sci.*, 2005, **288**,55.
8 C. Yan, G. Li, P. Xue, Q. Wei and Q. Li, *J. Hazard. Mater.*, 2010,**179**,721.
9 B. Volesky, *Water Res.*, 2007,**41**,4017.
10 K. A. Shroff, and V. K.Vaidya, *J. Chem. Technol. Biotechnol.*, 2012,**87**, 294.
11 Y. Bessekhouad, D. Robert, and J. V. Weber, *J. Photochem. Photobiol. A*, 2004, **163**, 569.
12 F. Schurz, J. M. Bauchert, T. Merker, T. Schleid, H. Hasse and R. Glaser, *Appl. Catal. A*, 2009, **355**, 42.
13 K. Miyazaki, M. Hieda and T. Kato, *Ind. Eng. Chem. Res.*,1997, **36**, 88.
14 M. M. Thackeray, *Prog. Solid State Chem.*, 1997, **25**, 1.
15 W. Xiao, D. Wang and X. W. Lou, *J. Phys. Chem. C*, 2010, **114**,1694.
16 H. Guo, R. Mao, D. Tian,W. Wang,D. Zhao,X. Yang andS. Wang, *J. Mater. Chem. A*, 2013, **1**, 3652.
17 H. Guo,Y. He,Y. Wang,L. Liu,X. Yang,S. Wang,Z. Huang and Q. Wei, *J. Mater. Chem. A,* 2013, **1**, 7494.
18 H. Guo, Y.Guo, T. Li, W. Wang, W. Chen, J.Chen and L. Liu,*Green Chem.*, 2014, doi:10.1039/C4GC00065J.
19 H. Guo, W. Wang, L. Liu, Y. He, C. Li and Y. Wang, *Green Chem.*, 2013, **15**, 2810.
20 H. Guo, L. Liu, T. Li, W. Chen, Y. Wang and W. Wang, *Chem. Commun.*, 2014, **50**, 673.
21 S.P. Mishra, S.S. Dubey, D. Tiwari, *J. Colloid Interface Sci*., 2004, **279**, 61.
22 K. H. Kang, D. M. Lim and H. Shin, *Water Res.*, 2006, **40**, 903.
23 M.I. Zaman, S. Mustafa, S. Khan, B.S. Xing, *J. Colloid Interface Sci.*, 2009, **330**, 9.
24 R. X. Chen, J. G. Yu, and W. Xiao, *J. Mater. Chem. A*, 2013,**1**,11682.
25 S.B. Kanungo, S.S. Tripathy, Rajeev, *J. Colloid Interface Sci.*, 2004, **269**, 1.
26 Q. Su, B. Pan, S. Wan, W. Zhang, L. Lv, *J. Colloid Interface Sci.*, 2010, **349**, 607.
27 E. Kim, C. Lee, Y. Chang, Y. Chang, *ACS Appl. Mater. Interfaces,* 2013, **5**, 9628.
28 S. Chandra, P. Dasa, S. Bag, R. Bhar and P. Pramanika, Mater. Sci. Eng. B, 2012, **177**, 855.
29 M. L. Chacón-Patiño, C. Blanco-Tirado, J. P. Hinestrozab and M. Y. Combariza ,*Green Chem.*, 2013,**15**, 2920.
30 W. Zhang, Z. Yang, X. Wang, Y. Zhang, Z. Wen and S. J. Yang, *Catal. Commun.*, 2006, **7**, 408.
31 Z. F. Bian, J. Zhu, J. G. Wang, S. X. Xiao, C. Nuckolls, H. X. Li, *J. Am. Chem. Soc.*, 2012, **134**, 2325.
32 C. Karunakaran, and P. Gomathisankar, *ACS Sustainable Chem. Eng.* ,2013, dx.doi.org/10.1021/sc400195n .
33 M. Zhu, C. L. Farrow, J. E. Post, K. J. T. Livi, S. J. L. Billinge, M. Ginder-Vogel, D. L. G. Sparks, *Cosmochim. Acta* 2012, **81**, 39.
34 D. Sarkar, C. K. Ghosh, S. Mukherjee, K. K. Chattopadhyay, *ACS Appl. Mater. Inter.*, 2013, **5**, 331.
35 H. Gnayem, and Y. Sasson, *ACS Catal.*, 2013, **3**, 186.
36 X. Y. Kong, Y. Ding, R. Yang, Z. L. Wang, *Science*, 2004, **303**, 1348.
37 J. Wu, Z. M. Wang, V. G. Dorogan, S. Li, J. Lee, Y. I. Mazur, E. S. Kim, and G. J. Salamo, *Nanoscale Res. Lett.*, 2013, **8**, 5.
38 C. J. Jia, L. D. Sun, F. Luo, X. D. Han, L. J. Heyderman, Z. G. Yan, C. H. Yan, K. Zheng, Z. Zhang, and M. Takano, *J. Am. Chem. Soc.*, 2008, **130**, 16968.
39 X. Li, *J. Phys. Chem. C*, 2010, **114**, 15343.
40 Q. Sun, Q. Wang, P. Jena, J. Yu and Y. Kawazoe, *Phys. Rev. B: Condens. Matter Mater. Phys.*, 2004, **70**, 2454.
41 M. Benavente, L. Moreno and J. Martinez, *J. Taiwan. Inst. Chem. Eng.*, 2011,**42**,976.
42 C. J. Karin, T. F. Valfredo, C. M. L. Mauro, N. Ademir and A. R. Peralt, *J. Colloid. Interf. Sci.*, 2005,**291**,369.
43 G. Sheng, S. Wang, J. Hu, Y. Lu, J. Li, Y. Dong, and X. Wang, *Colloids Surf. A*, 2009, **339**, 159.
44 M. H. Karaoğlu, İ. Kula, and M. Uğurlu, *Clean-Soil, Air, Water*, 2013, **41**, 548.
45 R. Xie, H. Wang, Y. Chen and W. Jiang, *Environ. Prog. Sustainable Energy*, 2013,**32**, 688.
46 X. F. Sun, Z. Jing, H. Wang and Y. Li, *J. Appl. Polym. Sci.*, 2013,**129**, 1555.
47 E. Kusvuran, D. Yildirim, A. Samil, and O. Gulnaz, *Clean -Soil, Air, Water*, 2012, **40**, 1273.
48 L. Kang, M. Zhang, Z. Liu and K. Ooi, *Spectrochim. Acta, Part A*, 2007, **67**, 864.
49 R. M. Potter and G. R. Rossman, *Am. Mineral.*, 1979, **64**,1219.
50 D. C. Golden, C. C. Chen and J. B. Dixon, *Science*, 1986, **231**,270.
51 I. A. Zouboulis, K. N. Lazaridis and K. A. Matis, *J. Chem. Technol. Biotechnol.*, 2002, **77**, 958.
52 Y. B. Liu, Y. Q. Wang, S. M. Zhou, S. Y. Lou, L. Yuan, T. Gao, X. P. Wu, X. J. Shi and K. Wang, *ACS Appl. Mater. Interfaces*, 2012, **4**, 4913.
53 I. Langmuir, *J. Am. Chem. Soc.*, 1918, **40**, 1361.
54 H. M. F. Freundlich, *Z. Phys. Chem.*, 1906, **57**, 385.
55 B. H. Hameed, A. A. Ahamd and N. Aziz, *J. Chem. Eng.*, 2007,**133**, 195.
56 J. J. Fan, W. Q. Cai and J. G. Yu, *J. Chem.-Asian*, 2011, **6**, 2481.
57 K. V. Kumar and A. Kumaran, *J. Biochem. Eng.*, 2005, **27**, 83.

A graphical and textual abstract for the Table of contents entry

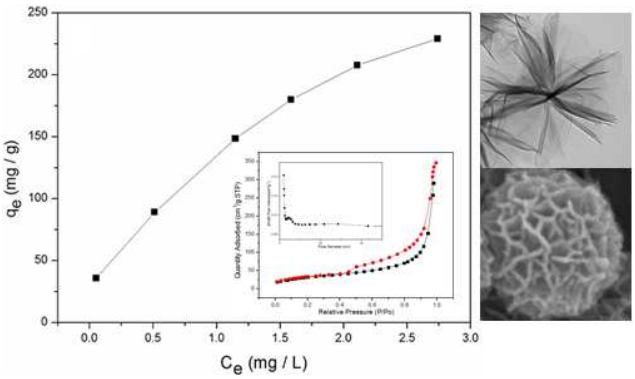

Hierarchical MnO_2 microspheres assembled by nano thin film are fabricated through an environmental route and subsequent dry under vacuum. The unique nano thin film assembly structure as well as the high BET surface area contributes greatly to the remarkable removal efficiency of heavy metal ions in water treatment.